JOURNAL OF VIROLOGY, Mar. 2010, p. 3004–3015 Vol. 84, No. 6
0022-538X/10/$12.00 doi:10.1128/JVI.02459-09

Mutations Abrogating VP35 Interaction with Double-Stranded RNA Render Ebola Virus Avirulent in Guinea Pigs▽

Kathleen C. Prins,[1]† Sebastien Delpeut,[2,3,4,5]† Daisy W. Leung,[6] Olivier Reynard,[2,3,4,5] Valentina A. Volchkova,[2,3,4,5] St. Patrick Reid,[1,2,3,4,5] Parameshwaran Ramanan,[6,7] Washington B. Cárdenas,[8] Gaya K. Amarasinghe,[6] Viktor E. Volchkov,[2,3,4,5]* and Christopher F. Basler[1]*

Department of Microbiology, Mount Sinai School of Medicine, New York, New York 10029[1]; Laboratoire des Filovirus, Inserm U758, 21 av. Tony Garnier, Lyon F-69007, France[2]; Université de Lyon, Lyon F-69007, France[3]; Université Lyon 1, Villeurbanne F-69622, France[4]; IFR 128 BioSciences Gerland-Lyon Sud, Lyon F-69007, France[5]; Department of Biochemistry, Biophysics and Molecular Biology, Iowa State University, Ames, Iowa 50011[6]; Biochemistry Graduate Program, Iowa State University, Ames, Iowa 50011[7]; and Laboratorio de Biomedicina, FIMCM, ESPOL, P.O. Box 09-01-5863, Guayaquil, Ecuador[8]

Received 20 November 2009/Accepted 17 December 2009

Ebola virus (EBOV) protein VP35 is a double-stranded RNA (dsRNA) binding inhibitor of host interferon (IFN)-α/β responses that also functions as a viral polymerase cofactor. Recent structural studies identified key features, including a central basic patch, required for VP35 dsRNA binding activity. To address the functional significance of these VP35 structural features for EBOV replication and pathogenesis, two point mutations, K319A/R322A, that abrogate VP35 dsRNA binding activity and severely impair its suppression of IFN-α/β production were identified. Solution nuclear magnetic resonance (NMR) spectroscopy and X-ray crystallography reveal minimal structural perturbations in the K319A/R322A VP35 double mutant and suggest that loss of basic charge leads to altered function. Recombinant EBOVs encoding the mutant VP35 exhibit, relative to wild-type VP35 viruses, minimal growth attenuation in IFN-defective Vero cells but severe impairment in IFN-competent cells. In guinea pigs, the VP35 mutant virus revealed a complete loss of virulence. Strikingly, the VP35 mutant virus effectively immunized animals against subsequent wild-type EBOV challenge. These *in vivo* studies, using recombinant EBOV viruses, combined with the accompanying biochemical and structural analyses directly correlate VP35 dsRNA binding and IFN inhibition functions with viral pathogenesis. Moreover, these studies provide a framework for the development of antivirals targeting this critical EBOV virulence factor.

Ebola viruses (EBOVs) are zoonotic, enveloped negative-strand RNA viruses belonging to the family *Filoviridae* which cause lethal viral hemorrhagic fever in humans and nonhuman primates (47). Currently, information regarding EBOV-encoded virulence determinants remains limited. This, coupled with our lack of understanding of biochemical and structural properties of virulence factors, limits efforts to develop novel prophylactic or therapeutic approaches toward these infections.

It has been proposed that EBOV-encoded mechanisms to counter innate immune responses, particularly interferon (IFN) responses, are critical to EBOV pathogenesis (7). However, a role for viral immune evasion functions in the pathogenesis of lethal EBOV infection has yet to be demonstrated. Of the eight major EBOV gene products, two viral proteins have been demonstrated to counter host IFN responses. The VP35 protein is a viral polymerase cofactor and structural protein that also inhibits IFN-α/β production by preventing the activation of interferon regulatory factor (IRF)-3 and -7 (3, 4, 8, 24, 27, 34, 41). VP35 also inhibits the activation of PKR, an IFN-induced, double-stranded RNA (dsRNA)-activated kinase with antiviral activity, and inhibits RNA silencing (17, 20, 48). The VP24 protein is a minor structural protein implicated in virus assembly and regulation of viral RNA synthesis, and changes in VP24 coding sequences are also associated with adaptation of EBOVs to mice and guinea pigs (2, 13, 14, 27, 32, 37, 50, 52). Further, VP24 inhibits cellular responses to both IFN-α/β and IFN-γ by preventing the nuclear accumulation of tyrosine-phosphorylated STAT1 (44, 45). The functions of VP35 and VP24 proteins are manifested in EBOV-infected cells by the absence of IRF-3 activation, impaired production of IFN-α/β, and severely reduced expression of IFN-induced genes, even after treatment of infected cells with IFN-α (3, 19, 21, 22, 24, 25, 28).

Previous studies proposed that VP35 basic residues 305, 309, and 312 are required for VP35 dsRNA binding activity (26). VP35 residues K309 and R312 were subsequently identified as critical for binding to dsRNA, and mutation of these residues

* Corresponding author. Mailing address for Christopher F. Basler: Mount Sinai School of Medicine, Dept. Microbiology, Box 1124, 1 Gustave L. Levy Place, New York, NY 10029. Phone: (212) 241-4847. Fax: (212) 534-1684. E-mail: chris.basler@mssm.edu. Mailing address for Viktor E. Volchkov: Filovirus Laboratory, INSERM U758, University Claude Bernard Lyon-1, 21 av. Tony Garnier, 69365 Lyon, Cedex 07 France. Phone: 33 437282450. Fax: 33 437282459. E-mail: viktor.volchkov@inserm.fr.

† These authors contributed equally to this study.

▽ Published ahead of print on 13 January 2010.

impaired VP35 suppression of IFN-α/β production (8). *In vivo*, an EBOV engineered to carry a VP35 R312A point mutation exhibited reduced replication in mice (23). However, because the parental recombinant EBOV into which the mutation was built did not cause disease in these animals, the impact of the mutation on viral pathogenesis could not be fully evaluated. Further, the lack of available structural and biochemical data to explain how the R312A mutation affects VP35 function limited avenues for the therapeutic targeting of critical VP35 functions. Recent structural analyses of the VP35 carboxy-terminal interferon inhibitory domain (IID) suggested that additional residues from the central basic patch may contribute to VP35 dsRNA binding activity and IFN-antagonist function (30). However, a direct correlation between dsRNA and IFN inhibitory functions of VP35 with viral pathogenesis is currently lacking.

In order to further define the molecular basis for VP35 dsRNA binding and IFN-antagonist function and to define the contribution of these functions to EBOV pathogenesis, an integrated molecular, structural, and virological approach was taken. The data presented below identify two VP35 carboxy-terminal basic amino acids, K319 and R322, as required for its dsRNA binding and IFN-antagonist functions. Interestingly, these residues are outside the region originally identified as being important for dsRNA binding and IFN inhibition (26). However, they lie within the central basic patch identified by prior structural studies (26, 30). Introduction of these mutations (VP35 with these mutations is designated KRA) into recombinant EBOV renders this otherwise fully lethal virus avirulent in guinea pigs. KRA-infected animals also develop EBOV-specific antibodies and become fully resistant to subsequent challenge with wild-type (WT) virus. Our data further reveal that the KRA EBOV is immunogenic and likely replicates to low levels early after infection *in vivo*. However, the mutant virus is subsequently cleared by host immune responses. These data demonstrate that the VP35 central basic patch is important not only for IFN-antagonist function but also for EBOV immune evasion and pathogenesis *in vivo*. High-resolution structural analysis, coupled with our *in vitro* and *in vivo* analyses of the recombinant Ebola viruses, provides the molecular basis for loss of function by the VP35 mutant and highlights the therapeutic potential of targeting the central basic patch with small-molecule inhibitors and for future vaccine development efforts.

MATERIALS AND METHODS

Antibodies, plasmids, and other reagents. Monoclonal antibody 6C5 against the Zaire EBOV VP35 protein was generated in collaboration with the Mount Sinai Hybridoma Center and has been previously described (8). Monoclonal antihemagglutinin (anti-HA) and anti-FLAG (M2) and polyclonal anti-FLAG antibodies were purchased from Sigma (St. Louis, MO). Rabbit monoclonal anti-phospho-IRF-3 (S396) (4D4G) antibody was purchased from Cell Signaling Technologies, and rabbit polyclonal anti-IRF-3 antibody was purchased from Santa Cruz.

Mammalian expression plasmids for the Zaire Ebola virus VP35 and FLAG-RIG-I were previously described (8, 41). The VP35 double point mutant R319A/K322A (KRA) was generated by standard PCR-based methods and cloned into the mammalian expression plasmid pCAGGS (36). Firefly luciferase was cloned into pCAGGS. The pRL-TK *Renilla* luciferase expression plasmid was purchased from Promega (Madison, WI).

Poly(rI) · poly(rC) (pIC) Sepharose was generated as described previously (8). Recombinant human IFN-ß was purchased from Calbiochem (San Diego, CA).

Sequence analysis. VP35 sequences from Zaire Ebola virus (ZEBOV, AAD14582), Reston Ebola virus (REBOV, AB050936), Sudan Ebola virus (SEBOV, EU338380), and Marburg virus (MARV, Z12132) were aligned using CLUSTALW version 1.81 (49).

Cell lines and viruses. 293T cells and Vero cells were maintained in Dulbecco's modified Eagle's medium (DMEM), supplemented with 10% fetal bovine serum, at 37°C and 5% CO_2. Sendai virus strain Cantell (SeV) was grown in 10-day-old embryonated chicken eggs for 2 days at 37°C.

Poly(rI) · poly(rC)-Sepharose coprecipitation. HEK 293T cells were transfected with a 1:1 ratio of Lipofectamine 2000 to plasmid DNA in Opti-MEM medium (Gibco) at 37°C for 8 h with the indicated plasmids. Twenty-four hours posttransfection, cells were lysed in 500 μl of lysis buffer (50 mM Tris, pH 8, 1% NP-40, 280 mM NaCl, 0.2 mM EDTA, 2 mM EGTA, and 10% glycerol) supplemented with 1 mM orthovanadate, 1 mM dithiothreitol, and a cocktail of protease inhibitors (Roche). Clarified cell lysates were mixed with 25 μl of phosphate-buffered saline (PBS)-washed pIC-Sepharose suspension. Beads and cell lysates were incubated with rocking for 2 h at 4°C. The beads were washed six times with lysis buffer, resuspended in sodium dodecyl sulfate-polyacrylamide gel electrophoresis (SDS-PAGE) sample loading buffer, separated by 10% SDS-PAGE, and analyzed by Western blotting with the indicated antibodies.

EBOV transcription/replication assay. The EBOV transcription/replication assay was based on a previously described system (34). 293T cells were cotransfected by the calcium phosphate precipitation method with T7-driven expression plasmids encoding the EBOV Zaire NP, L, VP30, and VP35 proteins. Also transfected were a T7 RNA polymerase expression plasmid and a plasmid that expresses from a T7 promoter a Zaire EBOV "minigenome" which encodes a fused green fluorescent protein (GFP)-chloramphenicol acetyltransferase (CAT) reporter gene flanked by *cis*-acting sequences necessary for replication and transcription of the RNA by a reconstituted EBOV polymerase complex. Also transfected was a constitutively expressing firefly luciferase expression plasmid that served as a transfection control. At 36 h posttransfection, cells were lysed with reporter lysis buffer (Promega) and CAT and firefly luciferase reporter activities were determined. CAT activity was normalized to firefly luciferase activity. Minigenome reporter activation was expressed as percent activity relative to the positive-control reaction (250 ng of wild-type VP35 plasmid), which was set to 100%.

Reporter gene assays. The IFN antagonist function of WT versus KRA mutant VP35 was evaluated by a reporter gene assay. 293T cells were transfected by the calcium phosphate precipitation method with the indicated amounts of expression plasmid, with an ISG54-promoter or an IFN-β-promoter firefly luciferase reporter plasmid (400 ng), and a constitutively expressed *Renilla* luciferase reporter plasmid, pRLTK (200 ng). To induce reporter gene expression, cells were either cotransfected with 50 ng of RIG-I expression plasmid or infected with SeV at a multiplicity of infection (MOI) of 10. In cases of infection, 12 h posttransfection, cells were infected with SeV or mock infected for 1 h. Twenty-four hours posttransfection, the cell lysates were assayed with the Dual Luciferase reporter assay (Promega), and firefly luciferase activity was normalized to *Renilla* luciferase activity. The results were expressed as percent induction relative to the positive control (either SeV infected, empty vector transfected [no VP35], or RIG-I induced, empty vector transfected [no VP35]), which was set to 100%.

IRF-3 activation assay. 293T cells were transfected with empty vector or with plasmids expressing WT or KRA mutant VP35. Twelve hours posttransfection, cells were either mock infected or infected with SeV for 1 h. Twelve hours postinfection (p.i.), cells were lysed with NP-40 lysis buffer. Lysate protein concentration was determined by Bradford assay per manufacturer instructions (Bio-Rad), and equal amounts of lysate were separated by SDS-PAGE. Western blotting was performed using anti-phospho-IRF-3 (S396), anti-IRF-3 (total IRF-3), and anti-VP35 antibodies, and the results were quantified with ImageJ software.

IFN bioassay. Conditioned media from 293T-transfected, SeV-infected cells were centrifuged (1 min at 13,000 rpm) and then UV treated for 10 min. The media were then overlaid onto Vero cells preplated in a 96-well plate (Costar, Corning, NY). After 12 h of treatment, the Vero cells were infected with a GFP-expressing Newcastle disease virus (NDV-GFP) at an MOI of 6 for 1 h. Twenty-four hours postinfection, viral replication was assessed by fluorescence microscopy and was quantified as described previously (8). Recombinant human IFN-β was added to Vero cells in a series of dilutions 24 h prior to NDV-GFP infection to generate a standard curve.

Sample preparation, crystallization, structure determination, and analysis of the KRA VP35 IID mutant. The KRA VP35 IID protein was expressed and purified as described previously (30, 31). Initial conditions for crystallization were identified using a commercial screen (Hampton Research). Optimum conditions were identified by grid expansion using in-house generated reagents and

TABLE 1. Data collection, phasing, and refinement statistics

Statistic type	Result
Data collection	
Model	VP35 IID K319A/R322A
Space group	$P2_12_12_1$
Cell dimension	$a = 51.43$, $b = 66.07$, $c = 72.64$ $\alpha = \beta = \gamma = 90$
Energy (eV)/wavelength (Å)	12,666/0.979
Resolution (Å)[c]	36.32–1.70 (1.76–1.70)
R_{merge}[a] (%)	8.9 (58.5)
I/σ (*I*)	9.4 (2.8)
Completeness (%)	97.5 (88.3)
Redundancy	6.34 (4.96)
Refinement	
Resolution (Å)	36.32–1.70
No. of unique reflections	27,195
R_{work}/R_{merge}[b]	19.1/24.6
No. of atoms	2,169
No. of solvent sites	251
B-factors, protein (Å^2)	11.42
B-factors, water (Å^2)	29.22
RMS bond lengths (Å)	0.021
RMS bond angles (°)	1.72

[a] $R_{merge} = \Sigma_i\Sigma_j \| I_{ij} - \langle I_j \rangle \|/\Sigma_i\Sigma_j I_{ij}$, where i runs over multiple observations of the same intensity and j runs over all crystallographically unique intensities.

[b] $R_{work} = \Sigma \|\| F_{obs} \| - \| F_{calc} \|\|/\Sigma \| F_{obs} \|$, where $\| F_{obs} \| > 0$. R_{merge} was based upon 10% of the data randomly selected and not used in the refinement.

[c] Highest-resolution shell is shown in parentheses.

iterative diffraction screening using a Rigaku/MCS R-AXIS IV++ detector system mounted on a rotating-anode X-ray generator of monochromated Cu Kα radiation. Best crystals were grown at 25°C using the hanging drop vapor diffusion method with 7 mg/ml KRA VP35 IID protein. Crystals were soaked in a reservoir solution with 10% glycerol (wt/vol) and cryocooled by being plunged into liquid nitrogen. The final diffraction data for structure solution were collected at the Advanced Light Source (Beamline 4.2.2; Berkeley, CA) at 100 K (Table 1). Data were processed with d*TREK (40). Intensities were converted to structure factors using the CCP4 program TRUNCATE (1). Phases were determined using molecular replacement with the native wild-type structure of VP35 IID (Protein Data Bank code: PDB 3FKE [30]) by PHASER (42) from the CCP4 package (1). Refinement was performed with REFMAC5 with manual rebuilding with Coot (35). Water molecules were initially added using ARP/wARP (29, 39) in REFMAC5 if a peak greater than 3.0σ was present in Fourier maps with coefficients $(F_{obs} - F_{calc})e^{i}\alpha^{calc}$ and later manually inspected with Coot (15). The model was further refined using REFMAC5 with the MLKF residual function, bulk solvent scaling, and individual isotropic B factors. Translation-libration-screw (TLS) parameters were determined with the TLMSD server (38). The quality of the refined model was validated with the MOLPROBITY server (10, 11) and SFCHECK and PROCHECK (1). Final refinement statistics for structures are shown in Table 1. Electrostatic surface calculations were conducted using the Adaptive Poisson-Boltzmann Solver as implemented in PyMOL, and all structure figures were prepared with PyMOL (12).

Generation of the recombinant Ebola viruses. All recombinant plasmids containing full-length cDNA copies of EBOV were generated as described elsewhere (33). Amino acid substitutions R319A and K322A in VP35 (KRA VP35) were introduced into intermediate plasmid-cassette pKSN-4 by site-directed mutagenesis essentially as described in reference 33. An additional transcription unit encoding GFP was inserted between the NP and VP35 genes in pFL-EBOV/VP35KRA/GFP and pFL-EBOV/GFP as described elsewhere (33). Using a reverse genetic system for EBOV (51), four recombinant viruses were rescued in BHK T7 cells and then amplified in Vero E6 cells. The viruses were designated EBOVwt, EBOVwt/GFP, EBOV/VP35KRA, and EBOV/VP35KRA/GFP. These viruses also contained mutations in genes encoding VP24 (M71I, L147P, T187I) which provide a dramatic increase in EBOV pathogenicity for guinea pigs (51). To confirm the presence of the introduced mutations, viral RNA was isolated from culture medium of Vero E6 cells infected with either virus, and cDNA was generated and amplified by reverse transcription-PCR (RT-PCR) and then sequenced.

All experiments involving full-length genomes and infectious EBOV were carried out in the Jean Merieux P4 Center biosafety level 4 laboratory (BSL4) in Lyon, France.

Growth characteristics of the recombinant viruses. Vero E6 and 293T cells were infected with recombinant viruses at an MOI of 0.01. Samples of culture medium were harvested at different time intervals (days 3, 4, 5, and 6 postinfection) and analyzed by Western blotting using anti-EBOV antibody. Infection with viruses expressing GFP was monitored by fluorescence microscopy.

The relative virus infectivity was estimated by normalization of the infectious titers (50% issue culture infective dose [$TCID_{50}$]/ml) determined by virus titration on Vero E6 cells to the amount of viral proteins as quantified by Western blot analysis.

Analysis of virus replication in guinea pigs. The effect of the mutations in VP35 on pathogenicity of EBOV in Hartley guinea pigs (females, 3 weeks old, 6 to 10 animals per group) was investigated. Animals were infected intraperitoneally with 500 $TCID_{50}$ of either EBOVwt or EBOV/VP35KRA. For control, two guinea pigs were inoculated with DMEM (mock infected). At day 17, mock-infected and EBOV/VP35KRA-infected animals were intraperitoneally inoculated with 500 $TCID_{50}$ of EBOVwt. The progress of infection was monitored by measuring the weight and the temperature of the animals on days 0, 3, 5, 6, 7, 8, 9, 10, 12, 14, 17, 18, 19, 20, 21, 24, 25, 26, and 27 postinfection. Animals with severe symptoms of distress were euthanized, and samples of spleen, liver, and sera were collected. In addition, two animals from each group were euthanized on days 3 and 5 p.i., and samples of the organs and sera were collected. Liver samples were used for nested PCR analysis using the following primers: For1, 5′-ATCGGAATTTTTCTTTCTCATT; Rev1, 5′-ATGTGGTGGGTTATAATA ATCACTGACATG; For2, 5′-GTCAAAGCATTTCCTAGCAACATGATGG; and Rev2, 5′-ATAATAATCACTCACATGCATATAACA.

The presence of specific anti-EBOV antibodies in the sera of guinea pigs was measured by immunofluorescence analysis using Vero E6 cells transfected with plasmids expressing VP40 and NP of EBOV. Briefly, the cells were transfected with plasmids expressing EBOV proteins, and 24 h posttransfection the cells were fixed and permeabilized using methanol/acetone. The cells were incubated with sera (dilution 1/80) at 4°C and then with secondary polyclonal donkey anti-guinea pig antibody coupled with Alexa 555. Immunofluorescence analysis was performed by using an Axio Observer microscope (Zeiss) and metamorph software (Ropper Scientific).

Samples of liver and spleen of mock-, EBOVwt- and EBOV/VP35KRA-infected animals were analyzed by immunohistochemistry. Formalin-fixed tissues were processed and embedded in paraffin according to conventional methods. Tissue sections were then deparaffinized, rehydrated, rinsed, and placed in PBS containing 3% bovine serum albumin (BSA) for 20 min. Slides were then developed with the mouse monoclonal anti-EBOV VP40 antibody (1:100) according to conventional methods. Sections were counterstained with hematoxylin.

RESULTS

KRA mutant VP35 lacks dsRNA binding activity. We sought to test the hypothesis that basic residues located C terminal to the 305–312 region are critical for VP35 dsRNA binding and IFN-antagonist activity. Residues R322 and K319 were chosen for mutagenesis because these are among a few highly conserved basic residues in the C terminus of VP35s from different EBOV species (Fig. 1). Moreover, a recent structural study of the VP35 C-terminal IID shows that R322 directly contacts dsRNA and mutation of R319 alone leads to a 3- to 5-fold loss of dsRNA binding (30, 31a). To test for binding to dsRNA, pull-down by poly(I · C)-Sepharose of full-length wild-type (WT) and KRA mutant VP35 was assessed (Fig. 2A). Lysates of 293T cells expressing either WT or KRA mutant VP35 were incubated with poly(I · C)-Sepharose or control Sepharose [no poly(I · C)] beads. The precipitated material was then detected by Western blotting, using an anti-VP35 antibody. As previously described, WT VP35 precipitated with poly(I · C)-Sepharose but not with the poly(I · C)-free beads (8). In contrast, the KRA mutant VP35 failed to detectably bind to the poly(I · C)-Sepharose, despite the presence of higher concentrations of KRA mutant VP35 than of WT VP35 in the lysates

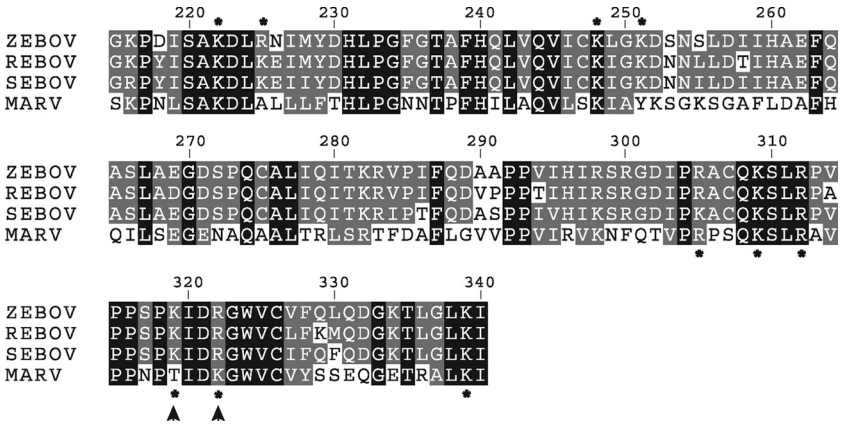

FIG. 1. Alignment of the amino acid sequences of the carboxy-terminal IIDs of Ebola and Marburg virus VP35s. Comparison of the filoviral VP35 IID sequences for Zaire EBOV, Reston EBOV, Sudan EBOV, and MARV. Residues that are completely conserved across all four sequences are highlighted in black, and residues that are identical or show high sequence similarity are highlighted in gray. Basic residues are highlighted with an asterisk, and K319 and R322 are indicated by arrowheads.

(Fig. 2A). Therefore, the KRA mutation renders VP35 defective for binding to dsRNA.

KRA mutant VP35 retains polymerase cofactor function. The relative activity of WT and KRA mutant VP35 as a polymerase cofactor was assessed using a "minigenome system" (Fig. 2B). In this assay, a model viral genome encoding a reporter gene is replicated by a viral RNA polymerase complex, which is reconstituted by transfection of expression plasmids for the viral NP, VP35, VP30, and L proteins (34). In the absence of VP35, no gene expression from the minigenome was detected (Fig. 2B). When WT VP35 plasmid was transfected, reporter gene expression was readily detected. In comparison, the KRA mutant VP35 yielded levels of activity similar to those of WT VP35 (Fig. 2B), demonstrating that KRA mutant VP35 retains function as a viral polymerase cofactor. The minor differences in activity of KRA and WT likely result from minor differences in protein expression levels.

KRA mutant VP35 exhibits impaired IFN antagonist function. Previously described VP35 dsRNA binding mutants exhibited reduced ability to suppress IRF-3 activation and IFN-α/β production (8, 26, 31a). Therefore, the efficiency with which KRA mutant VP35 can inhibit activation of an IRF-3-responive reporter gene was assessed. The KRA mutant VP35 was less effective than WT VP35 in suppressing Sendai virus-induced activation of the ISG54 promoter, a promoter that can be activated either by IRF-3 or by IFN-α/β (Fig. 2C). EBOV genomic RNA can activate RIG-I signaling, and WT VP35 can inhibit RIG-I-mediated activation of IRF-3 and transcription from the IFN-β promoter (8). Therefore, the efficiency with which KRA mutant VP35 can inhibit RIG-I-mediated activation of the IFN-β promoter was assessed by a reporter gene assay. Overexpression of RIG-I in 293T cells resulted in activation of the IFN-β promoter (Fig. 2D). Expression of WT VP35 suppressed this activation. However, KRA mutant VP35 failed to inhibit and in fact enhanced activation of the ISG54 promoter relative to the empty vector control (Fig. 2D). These data clearly demonstrate that the KRA mutation impairs inhibition of RIG-I signaling. Why KRA mutant VP35 increases the signal in this assay is uncertain, but it may reflect activation of the RIG-I pathway by transcripts expressed from the VP35 expression plasmids coupled with an inability of the KRA mutant VP35 to inhibit this activation.

To address the ability of WT versus KRA mutant VP35 to inhibit production of endogenous IFN-α/β, an IFN bioassay was employed (Fig. 2E). Cells transfected with empty vector, WT VP35, or KRA mutant VP35 were subsequently infected with Sendai virus at 1 day posttransfection. Cell supernatants were harvested 1 day postinfection, UV irradiated, serially diluted, and applied to preplated Vero cells. After overnight incubation, the Vero cells were infected with an IFN-α/β-sensitive green fluorescent protein (GFP)-expressing Newcastle disease virus (NDV-GFP), as previously described (8). GFP expression was quantified with a fluorescent plate reader 1 day postinfection with NDV-GFP. In this assay, WT VP35 suppressed IFN-α/β production relative to the empty vector control, whereas the KRA mutant VP35 failed to inhibit IFN-α/β production relative to the empty vector control. Supernatants from mock-infected cells had no detectable IFN-α/β as demonstrated by a maximal amount of NDV-GFP growth for all dilutions. It should be noted that the magnitude of inhibition by WT VP35 in this assay is limited by the presence of cells that remain untransfected with VP35 plasmid but which become infected with Sendai virus. Such cells will produce IFN-α/β without impediment by VP35. These results clearly demonstrate impaired capacity of the KRA mutant VP35 to inhibit production of endogenous IFN-α/β.

Previous studies demonstrated that VP35 inhibition of IFN-α/β production correlated with the capacity of VP35 to block phosphorylation of IRF-3 (3, 8). Therefore, the activation of IRF-3 was assessed in Sendai virus-infected cells transfected with empty vector, WT VP35, or KRA mutant VP35 by Western blotting for phospho-IRF-3 (Ser396). While WT VP35 suppressed the phospho-IRF-3 signal to near undetectable levels, significant levels of phospho-IRF-3 were present in cells transfected with the KRA mutant VP35 (Fig. 2F).

The KRA mutations do not perturb the structure of the interferon inhibitory domain of VP35 protein. Previous studies have shown that the VP35 dsRNA binding and IFN inhibitory functions map to the C-terminal IID (8, 30, 43) and that the VP35 IID alone is sufficient to inhibit IFN production (43). In

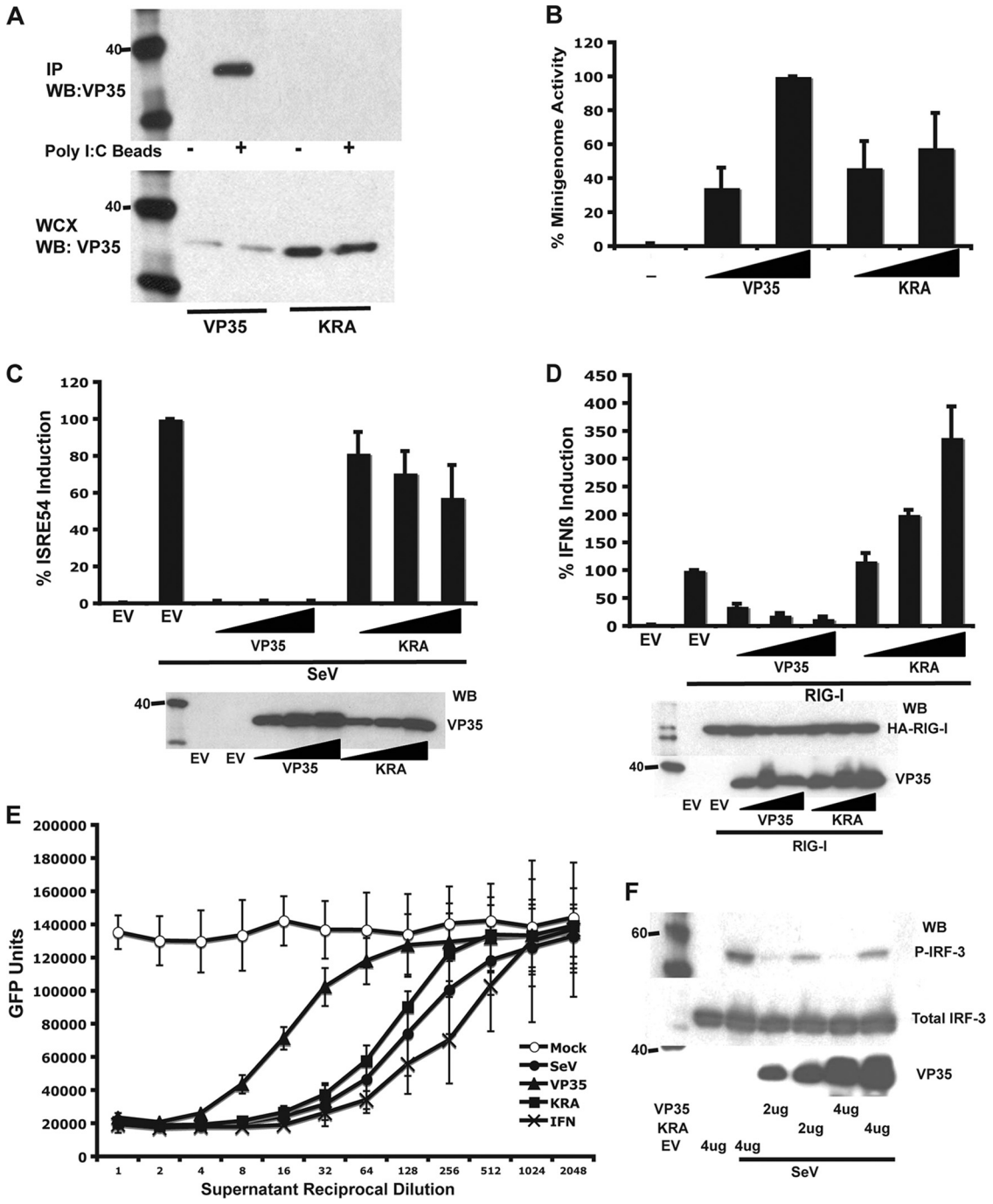

FIG. 2. KRA mutant VP35 lacks dsRNA binding and IFN antagonist activity but retains polymerase cofactor function. (A) Wild-type but not KRA mutant VP35 binds to poly(I · C)-Sepharose beads. WT or KRA mutant VP35 transfected cell lysates were incubated with poly(I · C) beads (+) or control Sepharose beads (−). The precipitated material was analyzed by Western blotting for VP35 (upper panel). Whole-cell extracts (WCX) were probed for VP35 (lower panel). (B) Polymerase cofactor activity of WT and KRA mutant VP35 was assessed with an EBOV minigenome assay. Wedges represent relative amounts of transfected WT or mutant VP35 expression plasmid. The value obtained with the higher concentration of WT VP35 was set to 100%. (C) WT and KRA mutant VP35 inhibition of SeV-induced ISG54 promoter activation. Cells were transfected with empty vector (EV) or increasing amounts (indicated by wedges) of WT VP35 or KRA mutant VP35 expression plasmid, an ISG54 promoter-firefly luciferase reporter plasmid, and a constitutively expressed *Renilla* luciferase reporter plasmid. Firefly luciferase activity was normalized to *Renilla* luciferase activity, and the activities of the EV-transfected and SeV-infected samples were set to 100% (top panel). Western blots show expression levels of WT and KRA mutant VP35 (lower panel). (D) WT and KRA mutant VP35 inhibition of RIG-I-induced IFN-β-promoter activation. Cells were transfected with empty vector (EV) or increasing amounts (indicated by wedges) of WT or KRA mutant VP35 expression plasmid, an IFN-β-promoter-firefly luciferase reporter plasmid, and a constitutively expressed *Renilla* luciferase reporter plasmid. Uninduced samples received additional empty vector DNA, and induced samples (RIG-I) received HA-tagged RIG-I expression plasmid. Firefly luciferase activity was normalized to *Renilla* luciferase activity, and the activities of the EV, RIG-I-transfected samples were set to 100% (top panel). Western blots (WB) show expression levels of WT and KRA mutant VP35 (lower panel). (E) IFN bioassay to assess suppression of

order to identify the structural basis leading to loss of dsRNA binding and corresponding loss of IFN inhibition, we examined by X-ray crystallographic and solution nuclear magnetic resonance (NMR) studies the perturbations caused by mutation of K319 and R322. To this end, we generated single crystals of KRA mutant VP35 IID protein, and X-ray diffraction data were generated as previously described (31). The structure of the KRA mutant VP35 IID was solved by molecular replacement using the WT VP35 IID as the search model (Table 1). As shown in Fig. 3A, limited structural changes occur at the secondary structure level, with a root mean square deviation (RMSD) value of <0.5 Å for the backbone residues compared to WT VP35 IID. In order to eliminate the potential effects of crystal packing and to gain further insight into the solution behavior of the mutant protein, we generated single and double mutants of VP35 IID proteins (K319A, R322A, and KRA) labeled with 1H/15N for solution NMR studies. As shown in Fig. 3B, the resulting two-dimensional heteronuclear single-quantum coherence (HSQC) spectra revealed a very good overlap between WT and mutant chemical shifts for the backbone amides, indicating that single and double mutations at K319 and R322 positions do not globally perturb the structure. Together, X-ray crystallographic and NMR data suggest that the KRA mutations do not cause structural perturbations beyond minimal local changes (up to 8 Å from the mutation site). In contrast to our structural observations, comparison of surface electrostatics between the WT and KRA mutant VP35 revealed noticeable differences, suggesting that changes in the surface electrostatics are likely responsible for the observed loss of dsRNA binding (Fig. 3C). These observations are also supported by the lack of differences in the hydrodynamic and oligomerization properties between the WT and KRA mutant VP35 IID proteins (data not shown).

Generation and analysis of recombinant viruses in cell culture. To investigate the effect of the KRA mutant VP35 on replication of EBOV, recombinant EBOVs were generated using a reverse genetics approach (51). Recombinant wild-type (EBOVwt) or KRA mutant VP35 (EBOV/VP35KRA) viruses were generated with or without an additional transcriptional unit encoding GFP. Furthermore, all recombinant viruses contained mutations in the VP24 gene. These VP24 mutations were shown to convert an EBOV originally apathogenic for guinea pigs into a virus that is highly lethal in guinea pigs (51). All recombinant viruses were rescued in BHK-T7 cells and then amplified in Vero E6 cells. Virus stocks were titrated by $TCID_{50}$ using Vero E6 cells. Two cell lines, Vero E6 and 293T cells, were used to compare multicycle growth kinetics of recombinant viruses (Fig. 4). Vero cells are known to be defective in IFN-α/β production, whereas 293T cells are IFN competent. Both cell types were infected with viruses at a multiplicity of infection (MOI) of 0.01 and monitored for several days postinfection. Samples of culture medium were collected at different intervals and analyzed by Western blotting. In addition, replication of recombinant EBOVwt/GFP and EBOV/VP35KRA/GFP was monitored by fluorescence microscopy. It appeared that both GFP-expressing viruses indistinguishably spread in Vero E6 cells as demonstrated by the kinetics of GFP distribution (Fig. 4A). Moreover, Western blot analysis of culture supernatants revealed that similar amounts of viral proteins were released with either virus (data not shown). In contrast, replication and spread of EBOV/VP35KRA/GFP in IFN-competent 293T cells were significantly affected by the mutations in VP35 (Fig. 4A). Weak GFP expression was observed in single 293T cells at days 3 and 4 postinfection, but there were no newly infected cells expressing GFP observed later postinfection. Importantly, EBOVwt/GFP replicated and spread in 293T cells (Fig. 4A) although with reduced kinetics compared to growth in Vero E6 cells, presumably due to the presence of a competent IFN system in these cells. The viruses containing no additional gene expressing GFP behaved similarly to those containing the GFP cassette (Fig. 4B). Western blot analysis of culture supernatants collected from the cells at different intervals showed that EBOVwt replicated in both Vero E6 and 293T cells, while EBOV/VP35KRA replicated well in Vero E6 cells but not in 293T cells due to the lack of release of viral proteins observed in these cells (Fig. 4B). Taken together, our data support the conclusion that the KRA mutation significantly impairs VP35 suppression of IFN-α/β responses with minimal effect on polymerase cofactor function as observed by the lack of replication in IFN-competent 293T cells but comparable replication in IFN-deficient Vero E6 cells when similar MOIs were tested. It should be noted that comparison of viral growth in Vero E6 cells by titration of culture supernatants and by assessing the amount of viral proteins released from the cells by Western blotting revealed that the wild-type and KRA mutant viruses exhibited different "infectivities." Similar quantities of viral proteins in the culture supernatants corresponded to markedly different infectious titers. Comparison of virus stocks prepared on Vero E6 cells by virus titration and Western blot analysis confirmed our observations made with 293T cells. Samples containing equal amounts of viral protein showed approximately 180 times fewer infectious units of EBOV/VP35KRA than of EBOVwt (Fig. 4C). The structure of surface GP was not affected by the introduced mutations, and therefore these two viruses should have no differences in their ability to infect the cells. Since Vero E6 cells are defective in IFN production, factors other than IFN production play a role in this phenomenon. Because of this difference, a greater amount of viral

endogenous IFN-α/β production by WT and KRA mutant VP35. Cells were transfected with 4 μg of empty vector (○ and ●), VP35 (▲), or KRA mutant VP35 (■) expression plasmids. Cells were mock infected (open symbol) or infected with SeV (solid symbols). Two-fold dilutions of UV-irradiated supernatants were applied to Vero cells. Direct treatment of Vero cells with dilutions of human IFN-β were included to generate a standard curve (×). Treated Vero cells were then infected with NDV-GFP, and virus replication was quantified with a fluorescence plate reader. (F) Inhibition of SeV-induced IRF-3 (S396) phosphorylation by WT and KRA mutant VP35. Cells were transfected with indicated amounts of empty vector (EV), WT, or KRA mutant VP35. Cells were mock infected or infected with SeV. Lysates were analyzed by Western blotting using anti-phospho-S396 IRF-3 (P-IRF-3) antibody (top panel), total IRF-3 antibody (middle panel), and an anti-VP35 antibody (lower panel). Error bars represent one standard deviation of results of at least three independent experiments.

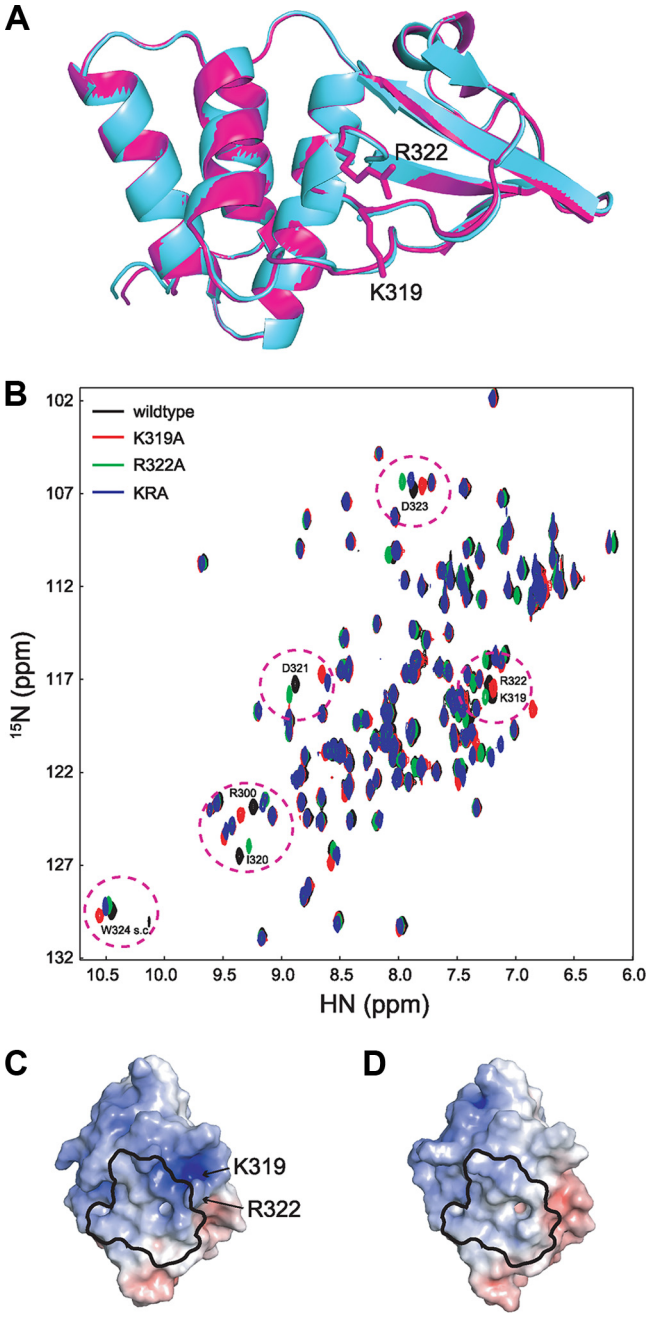

FIG. 3. Mutation of K319 and R322 does not significantly alter the structure of VP35 IID. (A) Alignment of WT VP35 IID (magenta, PDB 3FKE) and KRA mutant VP35 IID (cyan) crystal structures. (B) 1H/15N HSQC NMR spectrum overlay of WT and KRA mutant VP35 IID proteins showing localized chemical shift changes. Chemical shifts corresponding to WT, K319A, R322A, and KRA are colored black, red, green, and blue, respectively. Electrostatic surface potential (scale of -10 kT e^{-1} to $+10$ kT e^{-1}) of VP35 IID structures for wild-type (C) and KRA mutant (D) proteins. The dsRNA binding "footprint" is shown in black outline, and residues that are mutated are identified. Electrostatic potentials: blue, positive; white, neutral; red, negative.

protein is required of EBOV/VP35KRA than of EBOVwt to achieve equal multiplicities of infection.

Impact of KRA VP35 mutation on EBOV pathogenesis. To investigate the effect of KRA mutant VP35 on virus pathogenesis, groups of guinea pigs were inoculated intraperitoneally with 500 infectious units ($TCID_{50}$) of EBOVwt or EBOV/VP35KRA (Fig. 5B and C). Disease progression was monitored by measuring the weight and body temperature of the animals. At days 3 and 5 postinfection, two animals infected with EBOV/VP35KRA or EBOVwt virus were euthanized, and samples of the liver, spleen, and blood were collected for analyses. Mock-infected animals exhibited continual weight gain (Fig. 5A, top right panel). Weight loss of EBOVwt-infected animals began on day 3 postinfection and progressed until the animals died or were sacrificed upon reaching an established humane endpoint on day 6 to 7 postinfection (Fig. 5A, middle right panel). An increase in body temperature was observed in these animals and inversely correlated with weight loss (Fig. 5A, middle panels). At the late stages of disease, all animals exhibited a significant decrease in body temperature. In contrast, EBOV/VP35KRA-infected animals did not exhibit any weight loss (Fig. 5A) or symptomatic changes in body temperature (Fig. 5A, bottom left panel). Indeed, the weight of these animals increased steadily postinfection at a rate similar to that for mock-infected animals (Fig. 5A, bottom right panel). We failed to detect the presence of EBOV RNAs (data not shown) or expression of EBOV VP40 in the liver or spleen of guinea pigs infected with EBOV/VP35KRA on day 3 and 5 postinfection, while the samples of EBOVwt-infected animals were found to be EBOV-antigen positive (Fig. 5C). In order to investigate whether guinea pigs inoculated with EBOV/VP35KRA developed an immune response against the viral infection, serum samples were collected on day 17 postinfection, and these animals were then challenged with 500 $TCID_{50}$ of EBOVwt. Weight loss was observed in two control animals originally inoculated with tissue culture medium (DMEM) and then challenged with EBOVwt. These animals exhibited signs of severe distress on day 6 to 7 postinfection and were humanely euthanized (Fig. 5A, top panel). Remarkably, the animals originally inoculated with EBOV/VP35KRA and then challenged with EBOVwt did not show any disease symptoms and continued to gain weight until they were euthanized on day 28 post-initial infection (Fig. 5A, bottom panel). Immunofluorescence (IF) analysis of serum samples was performed using cells expressing EBOV NP and VP40 (Fig. 5B). These two proteins were chosen for analysis since the antibodies directed against both proteins are often detected in the blood of animals and human patients surviving EBOV infection. Sera taken from EBOV/VP35KRA-infected animals at day 17 postinfection revealed the presence of EBOV-specific antibodies. Anti-EBOV antibodies were not detected in the sera obtained from EBOVwt-infected animals on day 6 postinfection. Immunohistochemistry analyses of tissue samples collected from EBOVwt- and EBOV/VP35KRA-infected animals as well as those from either mock- or EBOV/VP35KRA-infected animals that were subsequently challenged with EBOVwt were performed. No viral antigen was detectable in tissues from EBOV/VP35KRA-infected animals or in animals first given EBOV/VP35KRA and then challenged with EBOVwt. In contrast, virus replication was observed in EBOVwt-infected and in mock-infected, EBOVwt-challenged animals. Altogether, these data demonstrate that KRA mutation of VP35 results in the severe attenuation of otherwise lethal infection. Moreover,

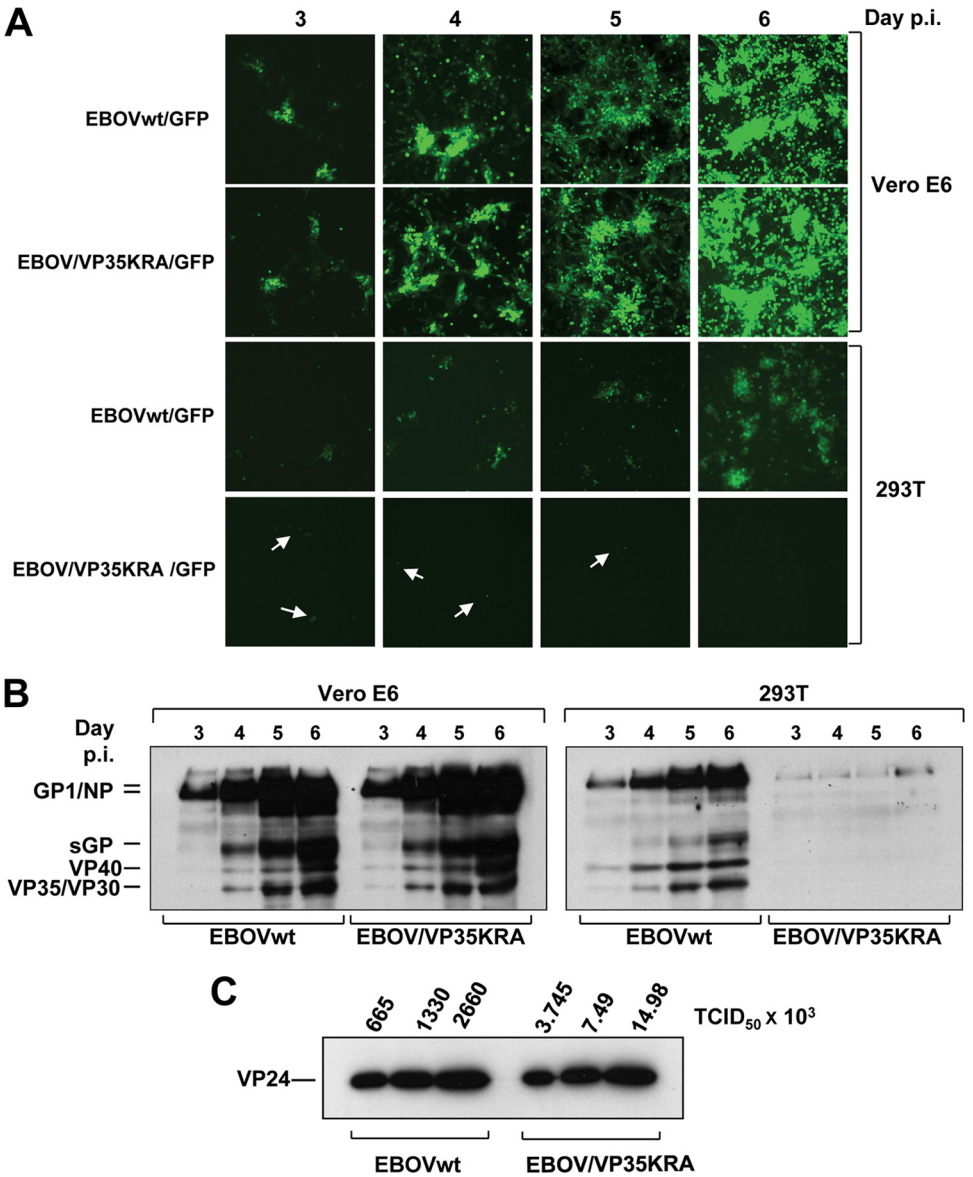

FIG. 4. Growth of EBOV/VP35KRA is strongly attenuated in 293T cells. Vero E6 and 293T cells were infected at an MOI of 0.01 with EBOVwt, EBOVwt/GFP, EBOV/VP35KRA, or EBOV/VP35KRA/GFP. (A) The replication of recombinant viruses expressing GFP was monitored using fluorescence microscopy on the indicated days postinfection (p.i.). Single GFP-expressing 293T cells observed after infection with EBOV/VP35KRA/GFP are indicated by arrows. (B) The culture medium from cells infected with either EBOVwt or EBOV/VP35KRA was harvested at different intervals postinfection and analyzed by Western blotting using polyclonal horse anti-EBOV antibodies. (C) Relative virus infectivity of virus stocks was estimated by normalization of the infectious titers ($TCID_{50}$/ml) determined by virus titration on Vero E6 cells to the amount of viral proteins as quantified by Western blot analysis using rabbit anti-VP24 antibody and goat anti-rabbit antibodies. EBOV/VP35KRA is less infectious than wild-type EBOV.

infection with VP35KRA EBOV protects the animals from EBOVwt challenge.

DISCUSSION

Despite significant interest in the mechanisms by which EBOVs cause severe disease, there is limited information linking specific structural features and specific molecular functions of viral gene products to virulence. Here, we conducted an integrated molecular, structural, and virological study, in order to gain insights into the molecular basis of VP35 function and to evaluate the structural basis of its role as a potential virulence factor. Previous structural studies of the C-terminal VP35 IFN inhibitory domain (IID) showed that VP35 IID forms a unique fold with an extended central basic patch comprised of Arg-305, Lys-309, Arg-312, Lys-319, Arg-322, and Lys-339 (30). Mutation of Arg-305, Lys-309, Arg-312, or a combination of these residues to alanine leads to decreased dsRNA binding and IFN suppression (8, 26). Further analyses suggested that additional residues, outside Arg-305, Lys-309, and Arg-312, may be important for function. However, the functional significance of these additional residues and their potential role in viral pathogenesis have not been previously

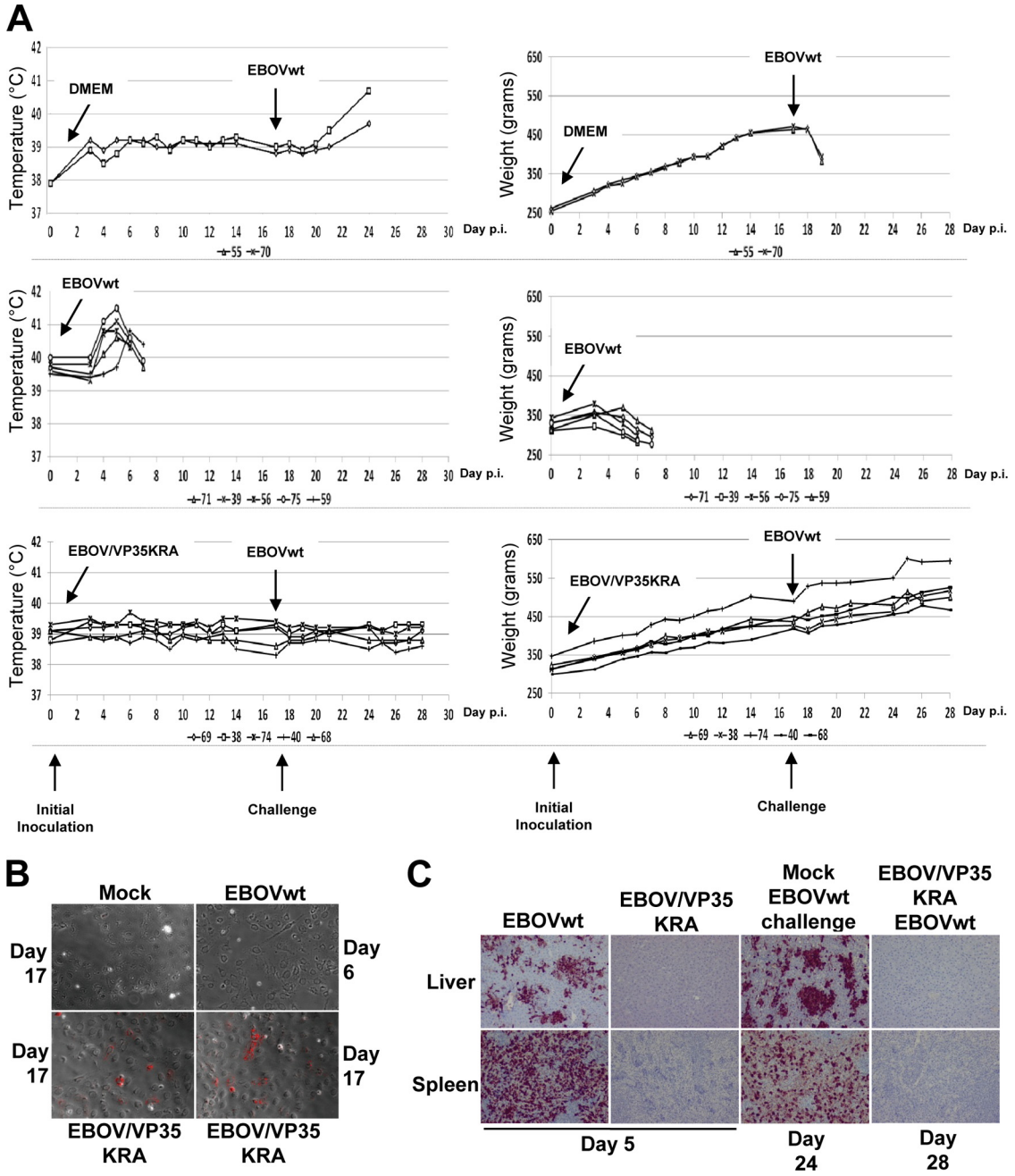

FIG. 5. EBOV/VP35KRA is highly attenuated in guinea pigs and protects against challenge with EBOVwt. (A) For the initial inoculation (on day 0), guinea pigs were mock infected (administered DMEM) (top panel) or inoculated intraperitoneally with 500 $TCID_{50}$ of either recombinant EBOVwt (middle panel) or recombinant EBOV/VP35KRA (bottom panel). On day 17 after the initial inoculation, animals were challenged with 500 $TCID_{50}$ of recombinant EBOVwt. Infections are indicated by labeled arrows. Animal weight was monitored for each animal on the indicated days postinfection (p.i.), and each animal is represented by an individual line. Legends under the graphs indicate a number designating individual animals. (B) Immunofluorescence analysis using sera from animals to stain Vero E6 cells transfected with plasmids expressing VP40 and NP of EBOV. Sera were collected from EBOVwt-infected animals on day 6 postinfection and from mock- and EBOV/VP35KRA-infected animals on day 17 postinfection. At 24 h posttransfection the cells were fixed and permeabilized using methanol/acetone. The cells were incubated with the sera from the animals as indicated and with secondary polyclonal donkey anti-guinea pig antibody coupled with Alexa 555. No specific anti-EBOV antibodies were detected in mock- or EBOVwt-infected animals. Animals infected with EBOV/VP35KRA showed specific anti-EBOV antibodies on day 17 postinfection. (C) Immunohistochemistry analysis of liver and spleen. Slides containing formalin-fixed tissues were processed and then stained using anti-EBOV VP40 mouse monoclonal antibody. EBOVwt-infected animals showed massive virus replication in liver and spleen. No specific staining was observed in tissues from EBOV/VP35KRA-infected animals.

examined. In order to address these questions and to correlate VP35 dsRNA and IFN inhibitory functions with pathogenesis, we examined the effects of the VP35 KRA mutant. To this end, we first analyzed the KRA mutant VP35 by X-ray crystallography, NMR spectroscopy, and biochemical methods. The data confirm that mutations at position 319 and 322 have little impact on the overall structure of the VP35 carboxy terminus but implicate the loss of surface charge in the failure to bind dsRNA and as a potential cause for the observed functional outcomes. Consistent with these findings, KRA mutant VP35 expressed in 293T cells was unable to detectably interact with dsRNA and, as predicted, the mutant VP35 was also impaired in its ability to suppress IRF-3 phosphorylation and reduced in its ability to inhibit IFN-α/β promoter activation and IFN-α/β synthesis. Collectively, these studies demonstrate that residues outside positions 305, 309, and 312, such as positions 319 and 322, play a critical role in dsRNA binding activity (8, 26) and suppression of IFN-α/β production (8, 23–25).

In the context of EBOV infection, loss of VP35 dsRNA binding and IFN antagonist functions results in severely impaired virus replication in cells capable of mounting an IFN-α/β response and also fully attenuates the virus *in vivo*. Using recombinant EBOVs, we now demonstrate that viruses encoding VP35KRA are unable to spread in IFN-competent cells. In contrast, the EBOV VP35KRA virus is able to replicate in IFN-defective Vero E6 cells. Interestingly, the attenuation of VP35KRA EBOV appears to be largely, but not exclusively, due to its impact on VP35 IFN-antagonist activity. In experiments using IFN-defective Vero E6 cells, growth differences between WT and KRA VP35 mutant virus were identified, although these were much smaller than the attenuation seen in 293T cells. Specifically, virus stocks produced in Vero E6 cells had reproducibly lower infectious titers for EBOV/KRA than for EBOVwt, even though the stocks contained similar amounts of viral proteins, suggesting an effect of mutations on virus "infectivity." In this regard, it appeared that this effect could be compensated for by adjusting the EBOV/KRA particle number such that a multiplicity of infection similar to that of EBOVwt was achieved. It is possible that other functions attributed to VP35, including its functions in virus structure, assembly, or innate immune evasion, also contribute to the attenuation of the KRA mutant (17, 20, 48). However, because the attenuation of virus replication was dramatically enhanced in 293T cells, which do produce IFN-α/β, it can be concluded that VP35-mediated evasion of host IFN-α/β responses is critical for efficient EBOV replication.

The critical role of residues K319 and R322 for EBOV pathogenesis was demonstrated in a unique guinea pig model. Although wild-type Zaire EBOV causes a nonlethal febrile illness in guinea pigs (5, 6, 46), past studies adapted Zaire EBOV to this species by repeated passage. This resulted in a uniformly lethal virus that causes a clinical syndrome similar to that observed in humans and nonhuman primates (5, 6, 9, 46). Importantly, guinea pig adaptation results in several genetic changes, relative to the parental strain, in several viral genes, including VP24 (50). In the present study, a parental virus was employed in which the introduction of only three amino acid changes to the VP24 protein is sufficient to permit lethal guinea pig infection. Complete characterization of these adaptive changes to VP24 and their role in guinea pig pathogenesis are the subject of separate studies. In this model, EBOV with wild-type VP35 causes massive virus replication and was detected in the liver and spleen by day 3 postinfection. The death of all animals was observed within 5 to 7 days postinfection. The mutant virus, on the contrary, was completely avirulent. The infection with EBOV/VP35KRA did not result in the development of any detectable disease symptoms, including fever and weight loss. Moreover, no viral RNA could be detected by reverse transcription-PCR (RT-PCR) (data not shown) nor were viral antigens detected in the liver or spleen at 3, 5, or 17 days or later postinfection, suggesting very low virus replication *in vivo*. In an attempt to assess whether EBOV/VP35KRA infects and replicates in guinea pigs, animals were challenged with lethal EBOVwt. Remarkably, each of the previously EBOV/VP35KRA-infected animals survived through 28 days postchallenge by EBOVwt. Given that the mutant virus appears to be cleared very soon after infection, these data suggest that infection with VP35KRA EBOV induced an anti-EBOV state protecting the animals from otherwise lethal EBOV WT infection. The presence of anti-EBOV antibodies in the EBOV/VP35KRA-infected animals indicates that sufficient levels of KRA viral antigens were expressed to induce an immune response. Given these observations, future experiments will determine whether clearance of the mutant virus and survival of the wild-type EBOV-infected animals require only an IFN-α/β response or whether additional immune functions also contribute to control of virus infection. Recently, it has also been demonstrated that a vesicular stomatitis virus that expresses EBOV glycoprotein (VSV-GP) is effective as a therapy when given postchallenge with Zaire EBOV (16, 18). We speculate that EBOV/VP35KRA may also exert a postexposure protective effect. If so, the basis for such a protective response may shed light on innate immune responses critical for control of EBOVs.

The present study is the first to directly correlate the structure and the specific molecular function of an EBOV protein with the lethality of the virus. Previous publications addressed the dsRNA binding activity of VP35 by a reverse genetics approach and a mouse animal model (26, 47). These authors demonstrated attenuation caused by a mutation at VP35 residue 312. However, the recombinant virus expressing wild-type VP35 did not result in lethal infection of these animals, leaving the impact of VP35 upon lethality open to further investigation. In this study, we demonstrate that mutations affecting anti-IFN activity of EBOV VP35 convert a highly pathogenic, lethal virus into an attenuated variant that causes no disease symptoms but does induce a protected state in the infected animals. Data obtained in this study may serve as a basis for structure-based antiviral strategies because specific structural features of VP35 were linked to functions essential for virulence. Consistent with the observations of this study, a recent analysis of the VP35 bound to dsRNA suggests a critical role for residues Lys-319 and Arg-322 (31a). In particular, Arg-322 makes direct contacts with dsRNA in the complex structure. Thus, correlations identified in this study between VP35 functions, dsRNA binding, and IFN inhibition and viral pathogenesis provide previously unidentified therapeutic targets. In this regard, it is interesting to note that there are several grooves or cavities as well as other charged patches within VP35 IID (30) that can be potentially targeted for antiviral development. Im-

portantly, examination of VP35 sequences from different EBOVs shows that the critical basic residues in the VP35 C terminus are highly conserved among EBOV variants as well as in the related Marburg virus (26, 47) (Fig. 1). Therefore, efforts to target the VP35 C terminus for anti-Ebola virus drug development may also provide a framework for development of panfiloviral therapeutics.

ACKNOWLEDGMENTS

All experiments involving live Ebola viruses were carried out in the INSERM BSL-4 laboratory Jean Merieux in Lyon, France. We thank the biosafety team members for their assistance in conducting experiments with infected animals. We thank D. Borek and J. Nix for assistance in diffraction data collection and model refinement. We also thank Charalampos Valmas for assistance in manuscript preparation.

This work was supported in part by funds from NIH grants AI059536 and AI057158 (Northeast Biodefense Center-Lipkin) to C.F.B., 1F32AI084324 to D.W.L., R01AI081914, a Developmental Grant (U54AI057160-Virgin [PI]) and funds from the Roy J. Carver Charitable Trust (09-3271) to G.K.A., and funds from INSERM (France), ANR, and Deutsche Forschungsgemeinschaft (SFB 593) to V.E.V. S.D. was supported by Délégation générale pour l'armement (DGA-CNRS 2005 170).

REFERENCES

1. **Acta Crystallogr. D Biol. Crystallogr.** 1994. The CCP4 suite: programs for protein crystallography. Acta Crystallogr. D Biol. Crystallogr. **50:**760–763.
2. **Bamberg, S., L. Kolesnikova, P. Moller, H. D. Klenk, and S. Becker.** 2005. VP24 of Marburg virus influences formation of infectious particles. J. Virol. **79:**13421–13433.
3. **Basler, C. F., A. Mikulasova, L. Martinez-Sobrido, J. Paragas, E. Muhlberger, M. Bray, H. D. Klenk, P. Palese, and A. Garcia-Sastre.** 2003. The Ebola virus VP35 protein inhibits activation of interferon regulatory factor 3. J. Virol. **77:**7945–7956.
4. **Basler, C. F., X. Wang, E. Muhlberger, V. Volchkov, J. Paragas, H. D. Klenk, A. Garcia-Sastre, and P. Palese.** 2000. The Ebola virus VP35 protein functions as a type I IFN antagonist. Proc. Natl. Acad. Sci. U. S. A. **97:**12289–12294.
5. **Bowen, E. T., G. Lloyd, W. J. Harris, G. S. Platt, A. Baskerville, and E. E. Vella.** 1977. Viral haemorrhagic fever in southern Sudan and northern Zaire. Preliminary studies on the aetiological agent. Lancet **i:**571–573.
6. **Bowen, E. T., G. S. Platt, G. Lloyd, R. T. Raymond, and D. I. Simpson.** 1980. A comparative study of strains of Ebola virus isolated from southern Sudan and northern Zaire in 1976. J. Med. Virol. **6:**129–138.
7. **Bray, M., and T. W. Geisbert.** 2005. Ebola virus: the role of macrophages and dendritic cells in the pathogenesis of Ebola hemorrhagic fever. Int. J. Biochem. Cell Biol. **37:**1560–1566.
8. **Cardenas, W. B., Y. M. Loo, M. Gale, Jr., A. L. Hartman, C. R. Kimberlin, L. Martinez-Sobrido, E. O. Saphire, and C. F. Basler.** 2006. Ebola virus VP35 protein binds double-stranded RNA and inhibits alpha/beta interferon production induced by RIG-I signaling. J. Virol. **80:**5168–5178.
9. **Connolly, B. M., K. E. Steele, K. J. Davis, T. W. Geisbert, W. M. Kell, N. K. Jaax, and P. B. Jahrling.** 1999. Pathogenesis of experimental Ebola virus infection in guinea pigs. J. Infect. Dis. **179**(Suppl. 1)**:**S203–S217.
10. **Davis, I. W., A. Leaver-Fay, V. B. Chen, J. N. Block, G. J. Kapral, X. Wang, L. W. Murray, W. B. Arendall III, J. Snoeyink, J. S. Richardson, and D. C. Richardson.** 2007. MolProbity: all-atom contacts and structure validation for proteins and nucleic acids. Nucleic Acids Res. **35:**W375–W383.
11. **Davis, I. W., L. W. Murray, J. S. Richardson, and D. C. Richardson.** 2004. MOLPROBITY: structure validation and all-atom contact analysis for nucleic acids and their complexes. Nucleic Acids Res. **32:**W615–W619.
12. **Delano, W. L.** 2002. The PyMol molecular graphics system. DeLano Scientific, San Carlos, CA.
13. **Ebihara, H., A. Takada, D. Kobasa, S. Jones, G. Neumann, S. Theriault, M. Bray, H. Feldmann, and Y. Kawaoka.** 2006. Molecular determinants of Ebola virus virulence in mice. PLoS Pathog. **2:**e73.
14. **Elliott, L. H., M. P. Kiley, and J. B. McCormick.** 1985. Descriptive analysis of Ebola virus proteins. Virology **147:**169–176.
15. **Emsley, P., and K. Cowtan.** 2004. Coot: model-building tools for molecular graphics. Acta Crystallogr. D Biol. Crystallogr. **60:**2126–2132.
16. **Feldmann, H., S. M. Jones, K. M. Daddario-DiCaprio, J. B. Geisbert, U. Stroher, A. Grolla, M. Bray, E. A. Fritz, L. Fernando, F. Feldmann, L. E. Hensley, and T. W. Geisbert.** 2007. Effective post-exposure treatment of Ebola infection. PLoS Pathog. **3:**e2.
17. **Feng, Z., M. Cerveny, Z. Yan, and B. He.** 2007. The VP35 protein of Ebola virus inhibits the antiviral effect mediated by double-stranded RNA-dependent protein kinase PKR. J. Virol. **81:**182–192.
18. **Geisbert, T. W., K. M. Daddario-DiCaprio, K. J. Williams, J. B. Geisbert, A. Leung, F. Feldmann, L. E. Hensley, H. Feldmann, and S. M. Jones.** 2008. Recombinant vesicular stomatitis virus vector mediates postexposure protection against Sudan Ebola hemorrhagic fever in nonhuman primates. J. Virol. **82:**5664–5668.
19. **Gupta, M., S. Mahanty, R. Ahmed, and P. E. Rollin.** 2001. Monocyte-derived human macrophages and peripheral blood mononuclear cells infected with ebola virus secrete MIP-1alpha and TNF-alpha and inhibit poly-IC-induced IFN-alpha in vitro. Virology **284:**20–25.
20. **Haasnoot, J., W. de Vries, E. J. Geutjes, M. Prins, P. de Haan, and B. Berkhout.** 2007. The Ebola virus VP35 protein is a suppressor of RNA silencing. PLoS Pathog. **3:**e86.
21. **Harcourt, B. H., A. Sanchez, and M. K. Offermann.** 1998. Ebola virus inhibits induction of genes by double-stranded RNA in endothelial cells. Virology **252:**179–188.
22. **Harcourt, B. H., A. Sanchez, and M. K. Offermann.** 1999. Ebola virus selectively inhibits responses to interferons, but not to interleukin-1beta, in endothelial cells. J. Virol. **73:**3491–3496.
23. **Hartman, A. L., B. H. Bird, J. S. Towner, Z. A. Antoniadou, S. R. Zaki, and S. T. Nichol.** 2008. Inhibition of IRF-3 activation by VP35 is critical for the high level of virulence of Ebola virus. J. Virol. **82:**2699–2704.
24. **Hartman, A. L., J. E. Dover, J. S. Towner, and S. T. Nichol.** 2006. Reverse genetic generation of recombinant Zaire Ebola viruses containing disrupted IRF-3 inhibitory domains results in attenuated virus growth in vitro and higher levels of IRF-3 activation without inhibiting viral transcription or replication. J. Virol. **80:**6430–6440.
25. **Hartman, A. L., L. Ling, S. T. Nichol, and M. L. Hibberd.** 2008. Whole genome expression profiling reveals that inhibition of host innate immune response pathways by Ebola virus can be reversed by a single amino acid change in the VP35 protein. J. Virol. **82:**5348–5358.
26. **Hartman, A. L., J. S. Towner, and S. T. Nichol.** 2004. A C-terminal basic amino acid motif of Zaire ebolavirus VP35 is essential for type I interferon antagonism and displays high identity with the RNA-binding domain of another interferon antagonist, the NS1 protein of influenza A virus. Virology **328:**177–184.
27. **Huang, Y., L. Xu, Y. Sun, and G. Nabel.** 2002. The assembly of ebola virus nucleocapsid requires virion-associated proteins 35 and 24 and posttranslational modification of nucleoprotein. Mol. Cell **10:**307.
28. **Kash, J. C., E. Muhlberger, V. Carter, M. Grosch, O. Perwitasari, S. C. Proll, M. J. Thomas, F. Weber, H. D. Klenk, and M. G. Katze.** 2006. Global suppression of the host antiviral response by Ebola- and Marburgviruses: increased antagonism of the type I interferon response is associated with enhanced virulence. J. Virol. **80:**3009–3020.
29. **Lamzin, V. S., and K. S. Wilson.** 1993. Automated refinement of protein models. Acta Crystallogr. D Biol. Crystallogr. **49:**129–147.
30. **Leung, D. W., N. D. Ginder, D. B. Fulton, J. Nix, C. F. Basler, R. B. Honzatko, and G. K. Amarasinghe.** 2009. Structure of the Ebola VP35 interferon inhibitory domain. Proc. Natl. Acad. Sci. U. S. A. **106:**411–416.
31. **Leung, D. W., N. D. Ginder, J. C. Nix, C. F. Basler, R. B. Honzatko, and G. K. Amarasinghe.** 2009. Expression, purification, crystallization and preliminary X-ray studies of the Ebola VP35 interferon inhibitory domain. Acta Crystallogr. Sect. F Struct. Biol. Cryst. Commun. **65:**163–165.

31a. **Leung, D. W., K. C. Prins, D. M. Borek, M. Farahbakhsh, J. M. Tufariello, L. Helgeson, P. Ramanan, J. C. Nix, Z. Otwinowski, R. B. Honzatko, C. F. Basler, and G. K. Amarasinghe.** 17 January 2010. Structural basis for dsRNA recognition and interferon antagonism by Ebola VP35. Nat. Struct. Mol. Biol. [Epub ahead of print.] doi:10.1038/nsmb.1765.

32. **Licata, J. M., R. F. Johnson, Z. Han, and R. N. Harty.** 2004. Contribution of Ebola virus glycoprotein, nucleoprotein, and VP24 to budding of VP40 virus-like particles. J. Virol. **78:**7344–7351.
33. **Martinez, M. J., N. Biedenkopf, V. Volchkova, B. Hartlieb, N. Alazard-Dany, O. Reynard, S. Becker, and V. Volchkov.** 2008. Role of Ebola virus VP30 in transcription reinitiation. J. Virol. **82:**12569–12573.
34. **Muhlberger, E., M. Weik, V. E. Volchkov, H. D. Klenk, and S. Becker.** 1999. Comparison of the transcription and replication strategies of Marburg virus and Ebola virus by using artificial replication systems. J. Virol. **73:**2333–2342.
35. **Murshudov, G. N., A. A. Vagin, and E. J. Dodson.** 1997. Refinement of macromolecular structures by the maximum-likelihood method. Acta Crystallogr. D Biol. Crystallogr. **53:**240–255.
36. **Niwa, H., K. Yamamura, and J. Miyazaki.** 1991. Efficient selection for high-expression transfectants with a novel eukaryotic vector. Gene **108:**193–199.
37. **Noda, T., P. Halfmann, H. Sagara, and Y. Kawaoka.** 2007. Regions in Ebola virus VP24 that are important for nucleocapsid formation. J. Infect. Dis. **196**(Suppl. 2)**:**S247–S250.
38. **Painter, J., and E. A. Merritt.** 2006. Optimal description of a protein structure in terms of multiple groups undergoing TLS motion. Acta Crystallogr. D Biol. Crystallogr. **62:**439–450.
39. **Perrakis, A., T. K. Sixma, K. S. Wilson, and V. S. Lamzin.** 1997. wARP: improvement and extension of crystallographic phases by weighted averaging of multiple-refined dummy atomic models. Acta Crystallogr. D Biol. Crystallogr. **53:**448–455.

40. **Pflugrath, J. W.** 1999. The finer things in X-ray diffraction data collection. Acta Crystallogr. D Biol. Crystallogr. **55:**1718–1725.
41. **Prins, K. C., W. B. Cardenas, and C. F. Basler.** 2009. Ebola virus protein VP35 impairs the function of interferon regulatory factor-activating kinases IKKepsilon and TBK-1. J. Virol. **83:**3069–3077.
42. **Read, R. J.** 2001. Pushing the boundaries of molecular replacement with maximum likelihood. Acta Crystallogr. D Biol. Crystallogr. **57:**1373–1382.
43. **Reid, S. P., W. B. Cardenas, and C. F. Basler.** 2005. Homo-oligomerization facilitates the interferon-antagonist activity of the ebolavirus VP35 protein. Virology **341:**179–189.
44. **Reid, S. P., L. W. Leung, A. L. Hartman, O. Martinez, M. L. Shaw, C. Carbonnelle, V. E. Volchkov, S. T. Nichol, and C. F. Basler.** 2006. Ebola virus VP24 binds karyopherin alpha1 and blocks STAT1 nuclear accumulation. J. Virol. **80:**5156–5167.
45. **Reid, S. P., C. Valmas, O. Martinez, F. M. Sanchez, and C. F. Basler.** 2007. Ebola virus VP24 proteins inhibit the interaction of NPI-1 subfamily karyopherin alpha proteins with activated STAT1. J. Virol. **81:**13469–13477.
46. **Ryabchikova, E., L. Kolesnikova, M. Smolina, V. Tkachev, L. Pereboeva, S. Baranova, A. Grazhdantseva, and Y. Rassadkin.** 1996. Ebola virus infection in guinea pigs: presumable role of granulomatous inflammation in pathogenesis. Arch. Virol. **141:**909–921.
47. **Sanchez, A., T. W. Geisbert, and H. Feldmann.** 2007. Filoviridae: Marburg and Ebola viruses, p. 1410–1448. *In* D. M. Knipe, P. M. Howley, et al. (ed.), Fields virology, 5th ed. Lippincott Williams and Wilkins, Philadelphia, PA.
48. **Schumann, M., T. Gantke, and E. Muhlberger.** 2009. Ebola virus VP35 antagonizes PKR activity through its C-terminal interferon inhibitory domain. J. Virol. **83:**8993–8997.
49. **Thompson, J. D., D. G. Higgins, and T. J. Gibson.** 1994. CLUSTAL W: improving the sensitivity of progressive multiple sequence alignment through sequence weighting, position-specific gap penalties and weight matrix choice. Nucleic Acids Res. **22:**4673–4680.
50. **Volchkov, V. E., A. A. Chepurnov, V. A. Volchkova, V. A. Ternovoj, and H. D. Klenk.** 2000. Molecular characterization of guinea pig-adapted variants of Ebola virus. Virology **277:**147–155.
51. **Volchkov, V. E., V. A. Volchkova, E. Muhlberger, L. V. Kolesnikova, M. Weik, O. Dolnik, and H. D. Klenk.** 2001. Recovery of infectious Ebola virus from complementary DNA: RNA editing of the GP gene and viral cytotoxicity. Science **291:**1965–1969.
52. **Watanabe, S., T. Noda, P. Halfmann, L. Jasenosky, and Y. Kawaoka.** 2007. Ebola virus (EBOV) VP24 inhibits transcription and replication of the EBOV genome. J. Infect. Dis. **196**(Suppl. 2)**:**S284–S290.